

24 to existing rice maps in the An Giang province, with a good agreement (higher than 81%). The
25 rice planted areas are retrieved from the maps and successfully validated with the official
26 statistics available at each province ($R^2=0.92$). These results show that the method is useful for
27 large scale early mapping of rice areas, using current and future C band wide-swath SAR data.

28

29 **I. INTRODUCTION**

30

31 Rice is the staple food for more than half of humanity. Global rice production has increased
32 continuously in the last half-century, since the Green Revolution. In the same period, the use of
33 chemical inputs, the introduction of modern high-yielding varieties with short growing cycles,
34 and the increased access to machinery and irrigation systems have led to a linear growth of the
35 crop yields (+0.05ton/ha/year) according to the FAO (Food and Agriculture Organization of the
36 United Nations 2009) as well as to an increase of the number of crops per year. This higher
37 cropping intensity (from single to double or triple crop) together with the conversion of non-
38 arable land to arable land have resulted in a drastic increase of rice harvested areas in the 60s
39 and 70s (+1.4Mha/year) which slowed down in the 80s and 90s (+0.46Mha/year) and has tended
40 to stabilize over the last ten years as a result of approaching the limits of land use and of
41 cropping intensity, however with a large inter-annual variability due to climatic conditions and
42 socio-economic factors. As both the increase in yield and in planted areas will be facing
43 limitations in the next decades, it is unlikely that rice production can keep increasing at the same
44 rate. Meanwhile, world population, and therefore demand for food, has increased linearly over
45 the last fifty years (+80M/year), and is projected to keep growing until around 2050 up to 9
46 billion inhabitants (United Nations Department of Economic and Social Affairs, Population

47 Division 2004). This conjuncture is prone to create tensions in food markets that could lead to
48 world food price crises - as in April 2008 when the price of rice has more than doubled in only
49 seven months - and eventually to famines. In this context of price instability and threatened food
50 security, tools to monitor rice production in real-time are highly needed by governments, traders
51 and decision makers.

52 Moreover, rice agriculture is strongly involved in various environmental aspects, from water
53 management to climate change due to the high emissions of methane. For this reason, a longer-
54 term inter-annual monitoring is also required in order to study the impact of the changes in rice
55 areas and in cultural practices that are likely to occur in the next years to face the economic and
56 environmental context.

57 Satellite remote sensing data offer a unique possibility to provide frequent and regional to
58 global-scale observations of the Earth over a long period (the lifespan of a satellite is around 10
59 years, and satellites are launched regularly to provide continuity in the data).

60
61 Optical sensors are seriously limited by frequent cloud cover in tropical and sub-tropical areas
62 where rice is grown in majority. A study combining agricultural census data and a large dataset
63 of Landsat TM imagery allowed producing maps of the distribution of rice agriculture in China
64 at a 0.5° spatial resolution (Frolking et al. 2002). However, to achieve the coverage of such a
65 large area with high-resolution (30m) optical images, a consequent amount of data (520 scenes)
66 had to be collected over a period of two years, which makes the method unsuitable for the
67 production of timely statistics or yearly results. Because of the need of a high temporal
68 observation frequency to get enough cloud-free images, a frequent global coverage can be
69 ensured only through the use of medium resolution (around 250m-1km) sensors, such as the

70 MODerate resolution Imaging Spectrometer (MODIS), VEGETATION, or the MEdium
71 Resolution Imaging Spectroradiometer (MERIS). The joint analysis of time-series of vegetation
72 and water indices derived from these sensors, such as the Normalized Difference Vegetation
73 Index (NDVI), the Enhanced Vegetation Index (EVI), or the Normalized Difference Water
74 Index (NDWI), also known as the Land Surface Water Index (LSWI), exhibits a specific
75 temporal behaviour during flooding of rice paddies and transplanting of rice plants. This feature
76 has been exploited to map the spatial distribution of rice agriculture at large scales in China
77 using VEGETATION (Xiao et al. 2002a; Xiao et al. 2002b) and MODIS (Xiao et al. 2005), and
78 in South and South-East Asia using MODIS (Xiao et al. 2006). Although these methods have
79 produced very valuable outputs, none of them allows the retrieval of planted areas without the
80 use of ancillary data. Indeed, because of the large number of mixed pixels at such spatial
81 resolutions, the fractional cover of rice in each pixel classified as rice had to be estimated
82 through the use of high-resolution Landsat TM imagery (Xiao et al. 2002b; Xiao et al. 2005).
83 Also, in (Xiao et al. 2006), the cropping intensity had to be derived from national agricultural
84 statistics datasets, and the rice distribution in the Mekong River Delta was not properly reported
85 according to the authors, probably because the flood pattern misleads the rice detection
86 algorithm. The spatio-temporal distribution of rice phenology in the Mekong River Delta has
87 been accurately estimated by an harmonic analysis of EVI time profiles from MODIS
88 (Sakamoto et al. 2006). However, this method is not able to discriminate rice from other crops or
89 vegetation types, and a prior identification of rice fields - e.g. by existing databases - is therefore
90 needed.

91 Radar imaging systems, contrarily to optical sensors, have an all-weather capacity. The radar
92 data are also well adapted to distinguish rice from other land cover types because of the specific

93 response of the radar backscattering of inundated vegetation. The interaction between a radar
94 electromagnetic wave and vegetation involves mainly three mechanisms: the volume scattering,
95 the scattering from the ground attenuated by the vegetation canopy, and the multiple scattering
96 between the volume and the ground. The last term brings a negligible contribution compared to
97 the two others in the usual case of vegetation growing over non-flooded soils. However, in the
98 case of flooded fields such as rice paddies, this term becomes dominant when the plants develop
99 because of the double-bounce between the plant stems (which are the dominant scatterers in the
100 volume) and the water surface. This has been demonstrated by theoretical models for the case of
101 C-band co-polarized (HH or VV) backscatter at 23° incidence angle (Le Toan et al. 1997; Wang
102 et al. 2005). This volume-ground interaction (double-bounce) is responsible for the first of the
103 two main properties of the rice backscatter: the backscattering intensity at polarizations HH and
104 VV show a significant increase during the vegetative phase, right after the low values of the
105 flooding stage, and then decrease slightly during the reproductive phase until harvest. This
106 backscatter increase in rice fields was generally observed from ERS, RADARSAT-1 or ASAR
107 to be superior to 8 dB, and sometimes much more (Chakraborty et al. 2005; Chen et al. 2007;
108 Kurosu et al. 1995; Shao et al. 2001). Scatterometer measurements on an experimental paddy
109 field in Japan have shown that this high backscatter increase is observed not only at C-band but
110 also at X-band and L-band (Inoue et al. 2002). For L-band however, other studies demonstrated
111 that in the case of mechanically planted fields, this increase is smaller (3-4 dB) except in specific
112 configurations of the plant rows (orientation and spacing) where resonant scattering leads to
113 extreme backscatter increases of more than 20 dB (Rosenqvist 1999). This dependence on the
114 plant row configuration limits the usefulness of L-band data for operational applications at wide-
115 scale.

116 The vertical structure of the rice plants is responsible for the second property of the rice
117 backscatter: the vertically polarized wave is more attenuated than the horizontally polarized
118 wave, and for that reason the ratio of the HH and VV backscatter intensities is higher than that
119 of most other land cover classes, reaching values around 6-7dB according to a joint analysis of
120 ERS and RADARSAT-1 data (Le Toan et al. 1997; Ribbes and Le Toan 1999) and to the
121 modelling of C-band HH and VV (Le Toan et al. 1997; Wang et al. 2005). The same is observed
122 at X-band (Le Toan et al. 1989).

123 The rice fields mapping methods based on SAR data that have been developed so far mainly rely
124 on these two properties of rice fields. The first property (high backscatter increase during rice
125 growing season) has been exploited in classification algorithms using the temporal change of co-
126 polarized backscatter as a classification feature, mostly at C-band, in various Asian countries
127 (Chen and McNairn 2006; Le Toan et al. 1997; Liew et al. 1998; Ribbes and Le Toan 1999).
128 The second property (high HH/VV polarization ratio) has led to the development of methods
129 using this polarization ratio as a classification feature, at C-band in Vietnam (Bouvet et al. 2009)
130 and at X-band in Spain (Lopez-Sanchez et al. 2010). All these rice mapping schemes have
131 proven effective but have been applied only at local scales, with high resolution (less than 50 m)
132 data. The use of these methods and data to map rice on larger areas (regional to continental
133 scales) would require the acquisition and processing of a dissuasive amount of high resolution
134 data. The existence of wide-swath sensors in current (ASAR, RADARSAT-2, PALSAR) or
135 future (Sentinel-1, RISAT-1) systems opens the way to the adaptation of these methods to
136 medium-resolution (50-100m) data for the mapping of rice areas at large scale. However, no
137 satellite wide-swath data with dual-polarization HH and VV capability is available so far, so
138 only the methods based on backscatter temporal change can be considered.

139 The present study aims at developing an operational method for the early assessment of rice
140 planted areas using medium-resolution wide-swath single-polarization SAR imagery, by
141 exploiting the outstanding temporal behaviour of rice backscattering. Because of the limitations
142 of L-band in mechanically planted fields and because of the absence of wide-swath sensors
143 operating at X-band, we choose to use C-band data. Section II describes the test site and the data
144 used in the study. The mapping method is developed in Section III. Section IV presents the
145 mapping results and their validation.

146

147 **II. SITE AND DATA**

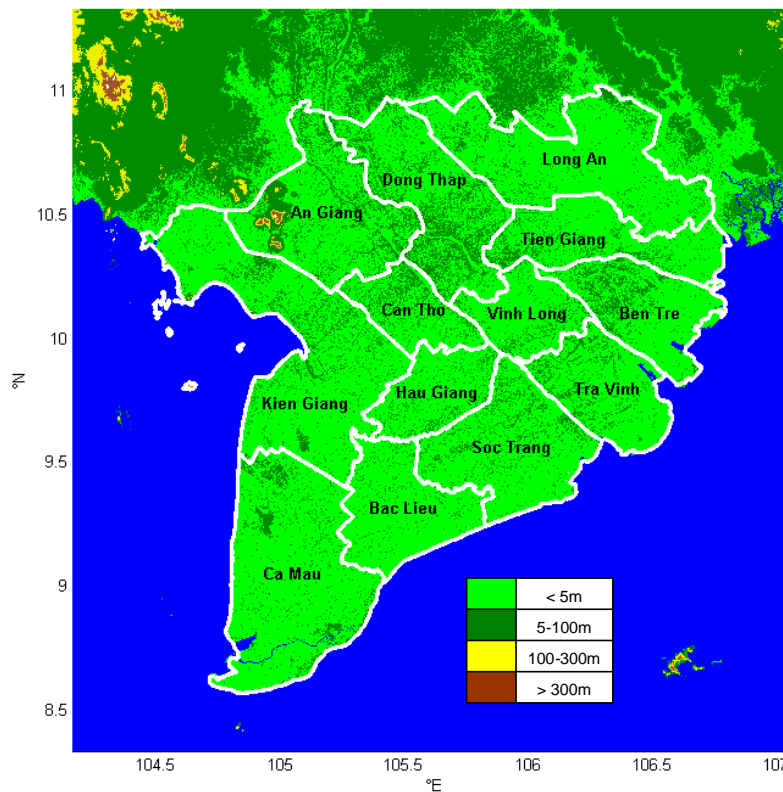
148

149 **A. Site description**

150 The study site is the Mekong Delta, the major rice-producing area in Vietnam. It produces more
151 than half of the rice in Vietnam, thus accounting for around 3% of the world production.

152 The Mekong Delta is a region constituted by 13 provinces in the southern tip of the country,
153 covering around 40000 km² (275km from North to South, 260km from West to East), where the
154 Mekong River approaches and empties into the South China sea through a network of nine main
155 distributaries. The topography is very flat, with most of the land below 5m. Figure 1 presents the
156 locations and names of the 13 provinces and the topography of the area from the Shuttle Radar
157 Topography Mission (SRTM) Digital Elevation Model (DEM). The climate is tropical (8.5°N-
158 11°N in latitude), with the wet season starting in May and lasting until October-November, and
159 the dry season from December to April. Seasonal floods occur in a large part of the area, starting
160 in August in the upper Delta, then spreading to the lower Delta, peaking in September-October
161 and lasting until the beginning of December. The floods bring large amounts of silt that

162 contribute to the fertilization of the soil. The land is dedicated mostly to agriculture (63%),
 163 aquaculture (17.7%) and forestry (8.9%) (General Statistics Office of Vietnam 2006), with the
 164 agricultural land comprising predominantly rice paddies (76%), as well as orchards, sugarcane
 165 and annual crops (General Statistics Office of Vietnam 2009). The delta is therefore a rural, but
 166 very densely populated area, with 17.7 million inhabitants.
 167



168
 169 Figure 1. Map of the 13 provinces in the Mekong River Delta and topography from SRTM.

170
 171 The rice cultivation pattern is quite complex. Originally, floating rice paddies were cultivated
 172 and, being dependent on rainfall and seasonal floods, only one crop of rice was harvested every
 173 year, during the wet season. However, in the last decades, the introduction of modern varieties,
 174 with higher yields and a shorter growth cycle, and technical components such as chemical

175 fertilizers, pesticides, machinery and low-lift pumps together with the development of canal
176 networks have led to the intensification of paddy agriculture, allowing to grow two or sometimes
177 three crops of rice per year (Tanaka 1995).

178 The land can be divided roughly into two ecological types: inland areas and coastal areas. Inland
179 areas are covered with a dense irrigation network and benefit from a fertile soil thanks to the
180 sediments brought by the floods, which allow double or triple-cropping of rice. They are formed
181 by inland provinces: An Giang, Đồng Tháp, Cần Thơ, Hậu Giang, Vĩnh Long, the western part
182 of Tiền Giang, and Long An. Coastal areas are prone to salt intrusion in the dry season which
183 limits the soil fertility. The major cropping patterns are therefore single rice with shrimp farming
184 or double rice. This concerns part or all of the coastal provinces: Kiên Giang, Cà Mau, Bạc Liêu,
185 Sóc Trăng, Trà Vinh and Bến Tre.

186
187 In inland areas, one crop of rice is grown during the dry season. This “Winter-Spring” rice
188 (locally called “Đông Xuân”) is planted in November-December and harvested between
189 February and April. In the wet season, farmers grow one or two crops of rice. The “Summer-
190 Autumn” crop (locally named “Hè Thu”) is planted in April-early June and harvested in July-
191 early August. When the fields are protected from seasonal floods (dykes have been built after the
192 2000 record floods), a second wet-season crop is grown. This “Autumn-Winter” rice (locally
193 named “Thu Đông”) is transplanted in August and harvested in November-December.

194 In coastal areas where saline intrusion limit the number of rice crops per year, one Summer-
195 Autumn rice is grown and a second crop in the “Main wet season” (locally called “Mùa”), which
196 is planted from July to August and harvested from November to February, i.e. with a variable
197 calendar between early, medium and late fields.

198 Table 1 sums up the information related to these seasons. Rice seasons are numbered according
199 to their order of occurrence in the civil year.

200

201 **Table 1. Rice agricultural seasons in the Mekong Delta River**

Season number	English name	Vietnamese name	Planting date	Harvest date	Distribution
1	Winter-Spring	Đông Xuân	Nov-Dec	Feb-Apr	inland
2	Summer-Autumn	Hè Thu	Apr-Jun	Jul-Aug	inland and coastal
3a	Autumn-Winter	Thu Đông	Aug	Nov-Dec	inland
3b	Main wet season	Mùa	Jul-Aug	Nov-Feb	coastal

202

203

204 **B. Statistical data**

205 The mapping methods developed in this paper will be validated through the comparison of the
206 planted areas retrieved from the remote sensing methods to the planted areas reported in the
207 official national statistical data.

208 The statistical system in Vietnam is centralized. Statistical data are collected first at the
209 commune level, and then aggregated at the district, province and finally country level by the
210 corresponding statistics offices. For obvious practical reasons, most of the agricultural statistics
211 are based on sampling at the district level, rather than on an exhaustive census. For the specific
212 case of rice planted areas, a three-stage sampling is applied in each district, at the commune,
213 village, and farming household levels. For the retained communes, enumerators report to the
214 District Statistics Offices the rice planted areas in the fields owned by the selected farming

215 households in the selected villages. The collected data are then forwarded to the Province
 216 Statistics Offices, and finally the General Statistics Office (GSO) (Food and Agriculture
 217 Organization of the United Nations 2002). Around 100000 farming households in the whole
 218 country are involved in the rice area sampling, out of a total of more than 9 million households
 219 that grow paddy (Food and Agriculture Organization of the United Nations 2002). This
 220 hierarchical acquisition scheme is very time- and resource-consuming. Moreover, its accuracy is
 221 intrinsically limited by the errors consecutive to the sampling.

222
 223 The General Statistics Office publishes annual agricultural statistics for each of the 58 provinces
 224 and 5 centrally-controlled municipalities in Vietnam. For paddy rice agriculture, these statistics
 225 comprise planted area, production and yield. The different crops of rice are gathered into three
 226 categories: Spring (labelled as “Đông Xuân” in the Vietnamese database), Autumn (“Hè Thu”)
 227 and Winter (“Mùa”) seasons. The figures for each of these three seasons in 2007 for every
 228 province of the Mekong River Delta are presented in Table 2.

229
 230 **Table 2. Planted area of rice by province for the three rice seasons in 2007 from national**
 231 **statistics**

	Planted area in 2007 (ha)		
	Spring	Autumn	Winter
Long An	234300	178800	15400
Tiền Giang	83400	163400	0
Bến Tre	20700	24200	34800
Trà Vinh	49700	81100	93200
Vĩnh Long	68500	89800	0

Đồng Tháp	208400	238700	0
An Giang	230600	282700	7300
Kiên Giang	265300	266500	51200
Cần Thơ	92100	115800	0
Hậu Giang	79000	110300	0
Sóc Trăng	140700	158900	25900
Bạc Liêu	33900	53300	62600
Cà Mau	0	36000	87100
Total	1506600	1799500	377500

232

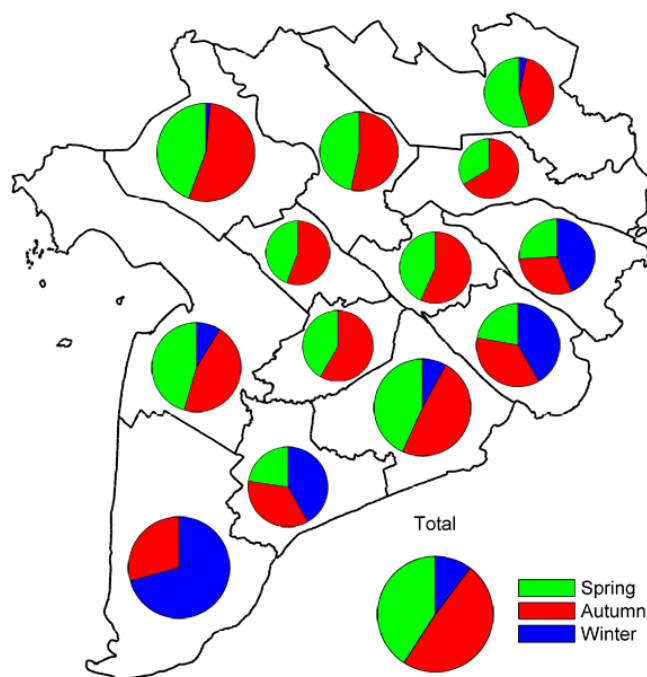
233

234 The correspondence between these three categories (Spring, Autumn, and Winter) and the
 235 agricultural seasons presented in the previous sub-section (Winter-Spring, Summer-Autumn,
 236 Autumn-Winter, and Main wet season) is not straightforward, and has to be discussed. The
 237 diversity of harvesting time and the differences in rice cropping patterns from the North to the
 238 South of Vietnam tend to make such a countrywide categorization irrelevant.

239

240 Figure 2 shows the proportion of each of the Spring, Autumn and Winter crops that are planted
 241 in each province in 2007 according to the statistics. The inland provinces grow mostly Spring
 242 and Autumn crops, with no or very few Winter crop, which seems paradoxical at first sight as
 243 triple-cropping is practised in these regions. The planted area for Autumn rice is higher than for
 244 Spring rice in the statistics, while in reality, the Winter-Spring and Summer-Autumn planted
 245 areas are similar, with the Autumn-Winter coming as an optional third crop in a small number of
 246 fields. Therefore, it can be assumed that in the inland provinces, the Spring statistical category
 247 accounts for the Winter-Spring crop, and the Autumn category for the sum of the Summer-

248 Autumn and Autumn-Winter crops. Reversely, the coastal provinces grow the three kinds of rice
 249 (except Cà Mau with no Spring rice), while the dominant patterns are single and double-
 250 cropping, with marginal areas growing irrigated triple-rice, especially in Soc Trang. It can then
 251 be inferred that, in the coastal provinces, the Spring category represents the Winter-Spring rice,
 252 the Autumn category corresponds to the Summer-Autumn rice and the Winter category gathers
 253 the main wet season (Mua) from the double-rice pattern and the Autumn-Winter season from the
 254 triple-rice pattern. Therefore, it seems that the three rice seasons described in the statistics do not
 255 cover the same categories in the coastal provinces and in the inland provinces. Table 3 gives a
 256 synthetic view of the supposed correspondence between these seasons from the statistical
 257 database and the agricultural seasons from Table 1.



258
 259 Figure 2. Proportion of Spring, Autumn and Winter rice planted in each province in 2007.

260

261 **Table 3. Correspondence between seasons from the statistical database and agricultural**
 262 **seasons.**

English name	Vietnamese name	Correspondence with agricultural seasons	
		Inland provinces	Coastal provinces
Spring	Đông Xuân	1	(1)
Autumn	Hè Thu	2 + 3a	2
Winter	Mùa	(3b)	(3a) + 3b

263

264

265 **C. ASAR APP rice seasons map for An Giang province data**

266 In a previous work (Bouvet et al. 2009), maps of the rice planted areas have been produced at a
 267 spatial resolution of 30m for the three rice seasons in 2007 in the province of An Giang. These
 268 maps have been obtained by applying a 3dB threshold on the polarization ratio HH/VV on a
 269 time-series of ASAR Alternating Polarization Precision image (APP) data at incidence IS2
 270 (19.2°-26.7°). The results have been validated using a land-use Geographic Information System
 271 (GIS) database covering one district, leading to a pixel-based accuracy of 89.9%. Moreover the
 272 estimated rice area in the Winter-Spring season for the whole province (229694 ha) has been
 273 compared to the preliminary statistics from the GSO (224273 ha), with a 2.4% difference
 274 between the two figures.

275 These maps will be used complementarily to the statistical data for further validation of the new
 276 methods presented in this paper.

277

278

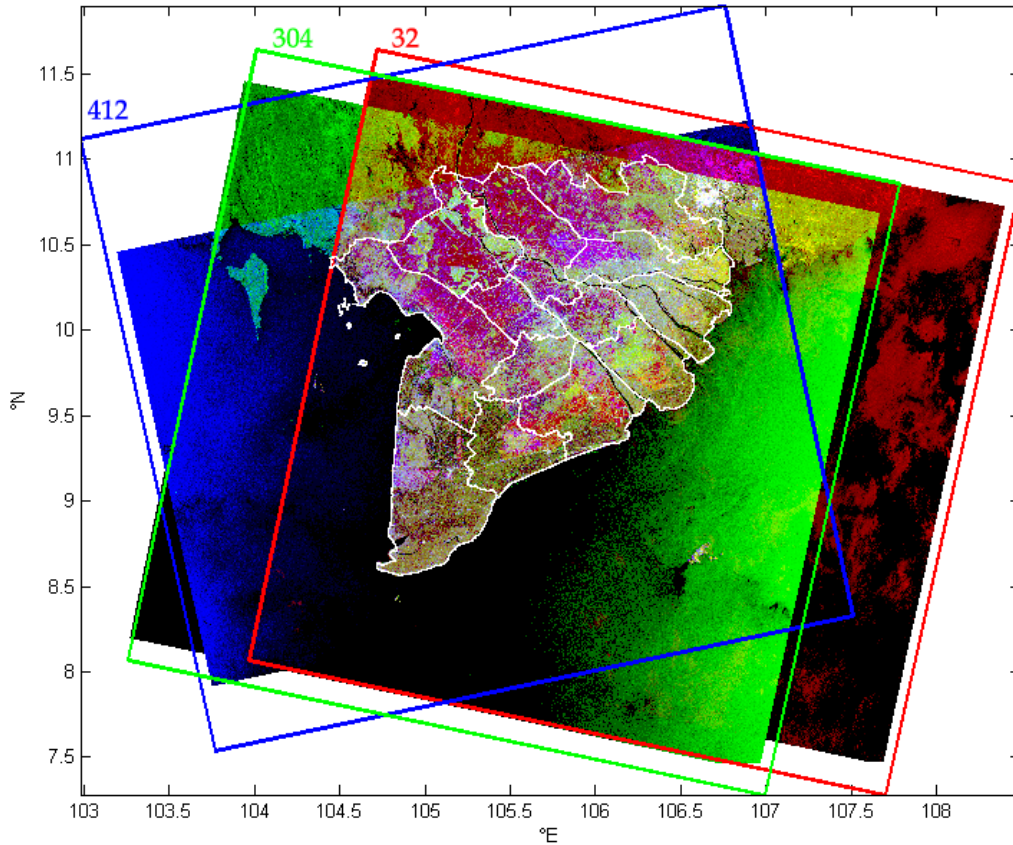
279 **D. ASAR WSM data**

280 The ASAR instrument is a C-band SAR instrument (5.6cm wavelength) onboard the European
281 satellite ENVISAT, which was launched in 2002, with multiple resolution, incidence, and
282 polarization ability. Among the five operating modes of ASAR (Image Mode, Alternating
283 Polarization, Wide Swath Mode, Wave Mode and Global Monitoring), only the Wide Swath
284 Mode, using the ScanSAR technique, offers a wide enough swath (around 400km) with a spatial
285 resolution adapted to accurate regional monitoring (around 150m, with a pixel spacing of 75m).
286 The incidence angle in each image ranges from 17° to 42°.

287 Extensive time-series of Wide Swath mode Medium resolution (WSM) data have been acquired
288 during the year 2007 over the Mekong Delta, with polarization HH, in order to monitor rice
289 agriculture by means of methods based on the backscatter temporal change.

290 Studies on the assessment of classification methods based on temporal change (Bouvet et al.
291 2010) and previous studies using RADARSAT (Ribbes and Le Toan 1999) have emphasized the
292 necessity of a high temporal observation frequency (e.g. around every ten days) to achieve
293 acceptable classification accuracy. The time lapse between repeat-pass orbits of ENVISAT is 35
294 days. In order to increase the observation frequency, data from three different satellite tracks
295 have been ordered: tracks 32 and 304 in descending pass and track 412 in ascending pass. Each
296 of the three tracks covers the delta entirely, as can be seen in Fig. 3. The other tracks that would
297 have covered the whole area have been left for the acquisition of Alternating Polarization data.

298



299

300

Figure 3. Colour-composite image of three WSM data from the three acquired tracks, with ascending tracks 32 and 304 in red and green respectively, and descending track 412 in blue.

301

302

The frames of the three tracks are presented in the corresponding colours.

303

304

The data acquisition sequence is the following: track 304, track 412, track 32 in intervals of

305

respectively 7 and 9 days, followed by the next sequence 19 days later. Therefore, in this three-

306

track configuration, the biggest time-lapse between two consecutive observations is 19 days,

307

with a mean acquisition interval of 11.7 days. The improvement is thus significant compared to

308

the single track acquisition frequency of one image every 35 days.

309 Table 4 lists the available dates for the three tracks. Track 412 is the most complete, with all the
 310 2007 satellite passes successfully acquired. The last acquisition for track 304 is missing, and the
 311 dataset for track 32 is incomplete, with only 6 acquisitions.

312

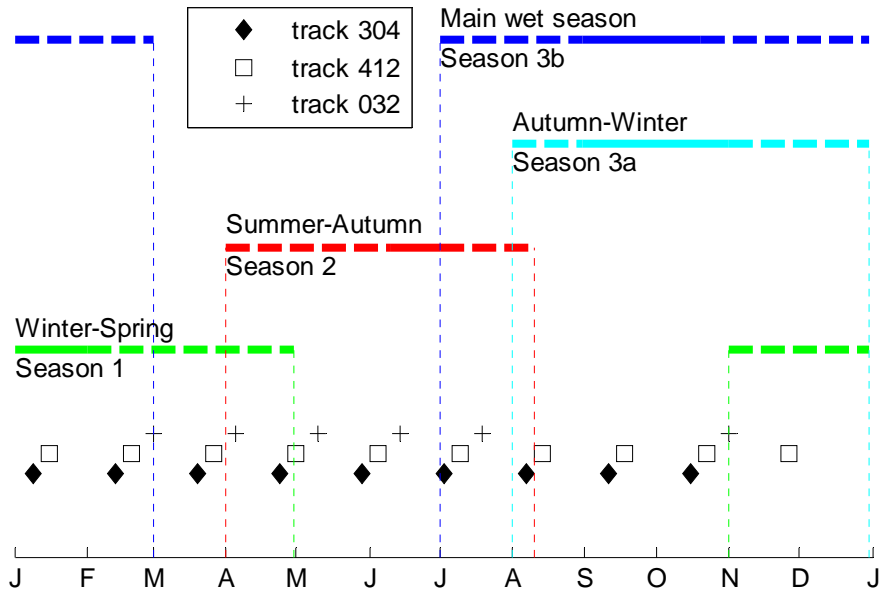
313 **Table 4. List of available dates in each track. Hyphens (-) indicate missing acquisitions.**

304	412	32
9 January	16 January	-
13 February	20 February	1 March
20 March	27 March	5 April
24 April	1 May	10 May
29 May	5 June	14 June
3 July	10 July	19 July
7 August	14 August	-
11 September	18 September	-
16 October	23 October	1 November
-	27 November	-

314

315 The acquisition dates of the three tracks are plotted in Fig. 4 together with the agricultural
 316 seasons of the rice calendar described in II.A

317



318

319

Figure 4. Rice calendar in the Mekong delta and dates of the available ASAR WSM data. For

320

each rice crop, dashed lines represent the periods during which the beginning and the end of the

321

crop can take place (spatial and interannual variability).

322

323

The conditions under which observations from different looking angles can be used together are

324

discussed in the next section.

325

The pre-processing of the WSM data is done with the Gamma GEO software (Gamma Remote

326

Sensing, Switzerland) and consists in the calibration of the SAR data and its geocoding with the

327

elevation data from the DEM of SRTM at 3 arcseconds, and projected to lat/lon coordinates at

328

the resolution of SRTM, corresponding to around 92m per pixel in latitude and longitude.

329

330

331

332

333

334 **III. MAPPING METHOD**

335

336 **A. Rationale**

337 The principle of this rice mapping method is to detect rice areas through the increase of their co-
338 polarized backscatter intensity between two repeat-pass acquisitions when the first acquisition
339 occurs at the flooding stage, i.e. when the backscatter is low because of the specular reflection
340 over water, and the second acquisition occurs when the rice plants have started to grow, i.e.
341 when the double-bounce provides high backscatter. Other classes are expected to remain
342 relatively stable in comparison. The method has already proven effective at 23° incidence and
343 HH or VV polarizations in past studies. The innovative aspect relies here in the use of multi-
344 track acquisitions to increase the observation frequency and in the use of wide-swath data to
345 ensure a regional coverage. For each pixel, the local incidence angle is different for the three
346 tracks, and within one image, the incidence angles varies from 17° in the near range to 42° in the
347 far range. The conditions under which such heterogeneous data can be used together have to be
348 examined so as to develop a classification method that is invariant to the temporal and spatial
349 variation in the incidence angle. The scatterometer measurements presented in (Inoue et al.
350 2002) and already mentioned in the introduction have been conducted at 25°, 35°, 45° and 55°
351 incidence. This study has shown that the value of C-band HH backscatter changes with the
352 incidence for a given phenological stage. A classification feature based on the value of the
353 backscattering intensity is thus unsuitable for the case of wide-swath data from different tracks.
354 For example, the detection of flooded fields by applying a threshold on the HH images to
355 identify the low backscatter areas would not be relevant because the threshold would have to
356 change with the local incidence angle within an image and between tracks. However, the

357 backscatter increase from flooding and transplanting to heading exceeds 9dB under any
358 incidence angle. A classification feature based on a measurement of the temporal increase of
359 backscatter between two consecutive acquisitions within a single track would therefore be
360 efficient to map rice regardless of the track and regardless of the location of the pixel in the
361 image. The temporal change is preferably measured by the ratio of intensities between two dates
362 (i.e. the difference in dB) rather than by the difference of intensities, the latter producing larger
363 classification errors in regions with a high backscatter than in regions with a low backscatter,
364 contrarily to the former for which the classification error is independent on the backscatter
365 intensity (Rignot and van Zyl 1993). Multi-track and multi-temporal classification features based
366 on the combination of temporal intensity ratios will therefore be developed in this paper for the
367 detection of rice fields.

368

369 **B. Algorithm description**

370 Computing the ratio of two SAR intensity images enhances the incertitude due to speckle. It is
371 therefore necessary to reduce the speckle noise before producing ratio images. In this study, the
372 backscatter images have been spatially filtered using an enhanced Lee filter (Lopes et al. 1990)
373 implemented in the ENVI software (ITT Visual Information Solutions), with a 5×5 window size.
374 The initial number of looks of the data is 3 in azimuth and 7 in range. The equivalent number of
375 looks, defined as $\text{mean}^2/\text{variance}$, is calculated to be around 12 in the geocoded WSM images,
376 and around 150 in the filtered images.

377 Figure 5 is a synoptic view of the different steps involved in the mapping algorithm, which will
378 be described in the following sub-sections.

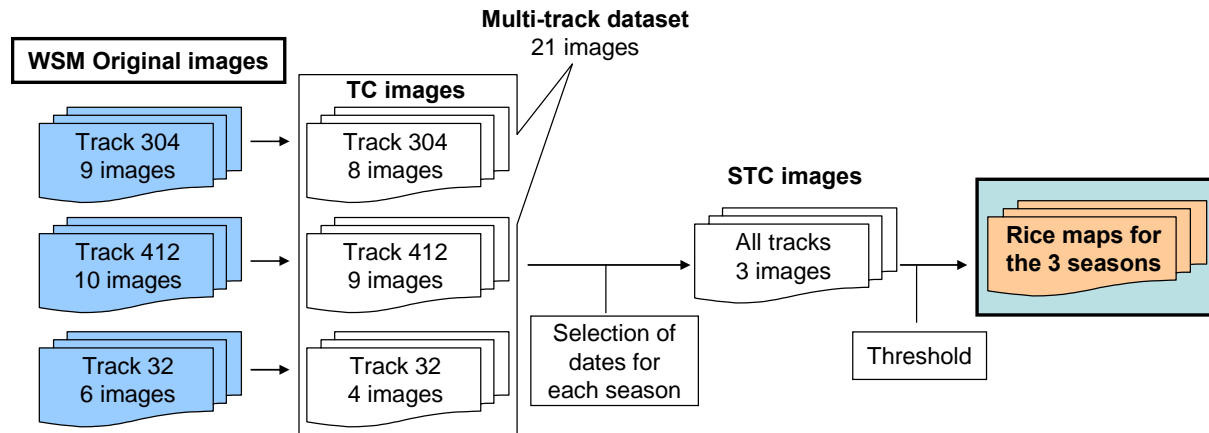


Figure 5. Synoptic view of the mapping algorithm.

Out of the twenty-five WSM images available in 2007, temporal change (TC) images are created by computing the ratio between two spatially filtered backscatter intensity images acquired within a track and separated by one satellite repeat pass (35 days): $TC = HH_{d+35} / HH_d$. These TC images compose a multi-track dataset of twenty-one images: eight from track 304, nine from track 412, and four from track 32.

The mapping algorithm consists in applying a threshold on these TC images in order to detect the rice fields that are flooded at the corresponding dates, characterized by their post-flooding backscatter increase. To detect all the rice areas planted during one season, one single TC image may however not be enough, because of shifts in the planting calendar, even within a province. The rice maps retrieved from the TC images must therefore be aggregated to produce seasonal maps. This is equivalent to applying the threshold directly on a seasonal temporal change (STC) classification feature, made up by taking the maximum value of the TC images among the dates corresponding to each season. The next sub-sections discuss how the threshold should be chosen, and how the dates corresponding to each season and each province can be selected. The

396 study will be conducted for Season 2 and Season 3 only, as the complete mapping of Season 1
 397 (Winter-Spring) would require data from the end of 2006.

398

399 **C. Defining the value of the classification threshold**

400 Under the assumption of gamma distributed SAR intensities and uncorrelated images, a
 401 theoretical expression of the optimal classification threshold t_{opt} can be found for the two-class
 402 problem - a rice class and a non-rice class - when the classification feature is a single TC image
 403 (Bouvet et al. 2010):

$$404 \quad t_{opt} = \sqrt{TC_{nr} TC_r} \cdot \frac{\sqrt{\frac{TC_r}{TC_{nr}} \left(\frac{p(nr)}{p(r)} \right)^{\frac{1}{2L}} - 1}}{\sqrt{\frac{TC_r}{TC_{nr}} - \left(\frac{p(nr)}{p(r)} \right)^{\frac{1}{2L}}}} \quad (1)$$

405 where nr and r denote respectively the non-rice and the rice classes, and $p(nr)$ and $p(r)$ denote the
 406 *a priori* probabilities of the non-rice class and of the rice class, i.e. the percentage cover of non-
 407 rice and rice in the landscape. TC_{nr} and TC_r represent the mean temporal change
 408 $\langle HH_{d+35} \rangle / \langle HH_d \rangle$ of the non-rice and the rice classes ($TC_r > TC_{nr}$), and L is the number of looks
 409 of the images (or the equivalent number of looks in case of filtered images). Ground-truth
 410 information is required to assess the values of $p(nr)$, $p(r)$, TC_{nr} and TC_r , and consequently the
 411 threshold t_{opt} to use in the classification. It is shown that the class parameters TC_{nr} or TC_r are
 412 linked by a simple relationship to $TC_{max,nr}$ and $TC_{max,r}$, which are the values where the
 413 probability density functions (pdf) of TC for the corresponding class is the highest, e.g. for the
 414 non-rice class:

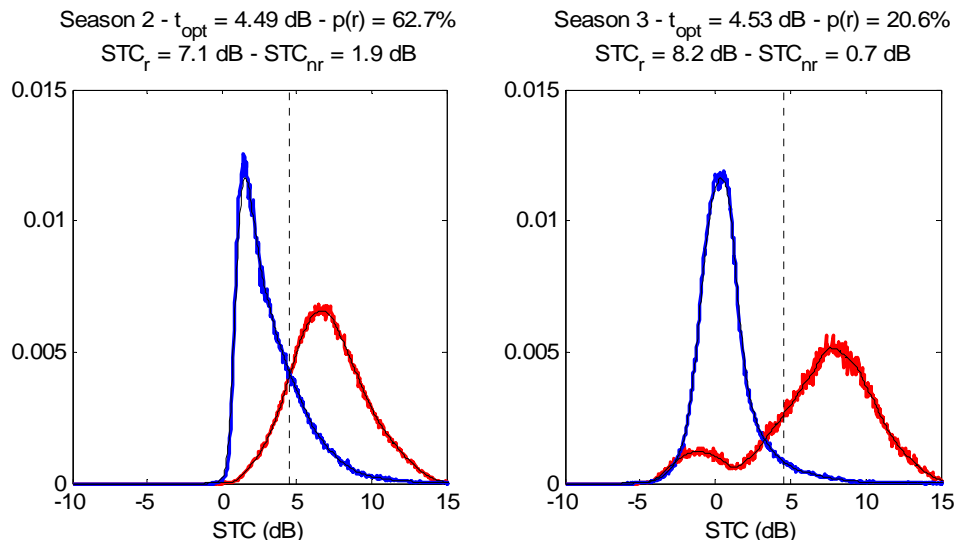
$$415 \quad TC_{nr} = \frac{L+1}{L-1} TC_{max,nr} \quad (2)$$

416 and likewise for the rice class.

417 For the case of STC images, equations (1) and (2) do not apply strictly because the pdf of STC is
418 different from the pdf of TC. However, as the pdf of STC cannot be expressed theoretically and
419 is not expected to differ much from that of TC, equations (1) and (2) will be used on the STC.

420 In the present study, the rice maps retrieved in (Bouvet et al. 2009) from the APP dataset can be
421 used as ground truth over the An Giang province to calculate $p(nr)$, $p(r)$, and to plot the
422 histograms of STC for the rice and the non-rice classes, for Season 2 (Summer-Autumn) and
423 Season 3 (Autumn-Winter), in order to estimate $STC_{max,nr}$ and $STC_{max,r}$. The proportion of rice
424 $p(r)$ calculated in the APP maps is 62.7% for Season 2 and 20.6% for Season 3. The normalized
425 histograms of these seasonal classification features are plotted in Fig. 6 for the two considered
426 classes, based on the pixels identified as rice or non-rice in the maps derived from APP, which
427 have been spatially degraded and projected to the geocoded WSM data. These normalized
428 histograms estimate the pdf of STC for the two classes. The STC_{max} parameters are assessed for
429 each class by identifying the STC value where the histogram is maximal, and the STC_r and
430 STC_{nr} class parameters are retrieved using equation (2). The values corresponding to the optimal
431 classification threshold t_{opt} for Summer-Autumn and Autumn-Winter are then found from (1) to
432 be respectively 4.49dB and 4.53dB.

433



434

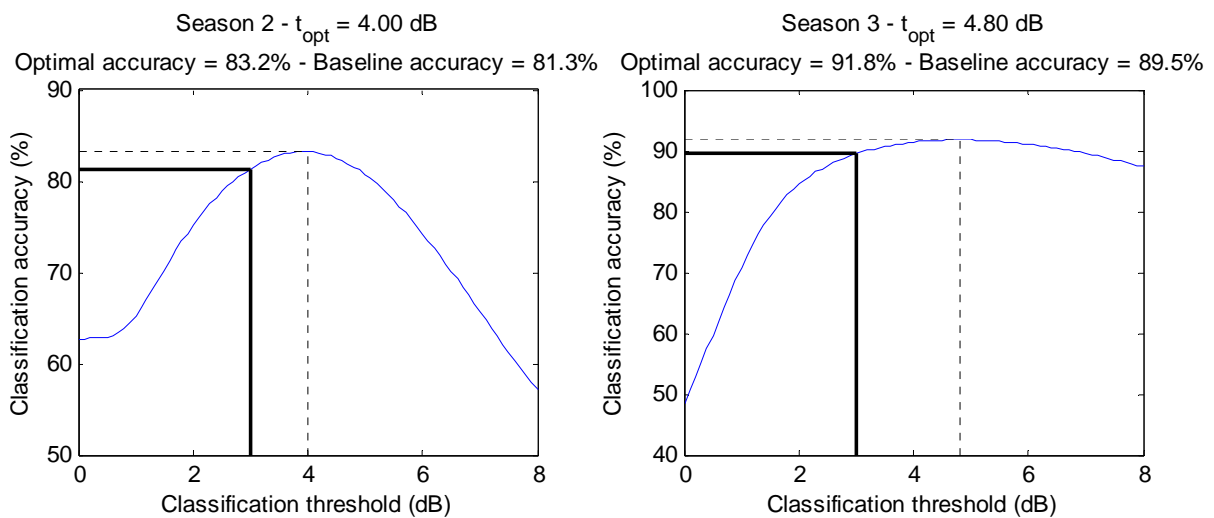
435 Figure 6. Histograms of the STC classification features for Season 2 (left) and Season 3 (right),
 436 for the rice class (red) and the non-rice class (blue). Vertical dashed black lines represent the
 437 theoretical optimal classification threshold t_{opt} retrieved from the histograms.

438

439 In most applications, no such extensive ground truth data is available. Quite commonly, the
 440 location of a few sample areas of rice and non-rice are known and allow an approximate
 441 estimation of STC_{nr} and STC_r . The class proportions, $p(nr)$ and $p(r)$, remain however generally
 442 unknown and have to be assumed to be equal to 0.5, which leads to a simplified expression of
 443 the optimal threshold: $t_{opt} = \sqrt{STC_{nr}STC_r}$. In less favourable cases when no ground
 444 information is available at all, like here in the other provinces of the Mekong delta, the
 445 theoretical value of the optimal classification threshold cannot be retrieved. In that case, the only
 446 option is to use values from literature. Previous studies have suggested a threshold of 3dB (Le
 447 Toan et al. 1997; Liew et al. 1998; Ribbes and Le Toan 1999), which can be used as a baseline
 448 algorithm. This value is significantly lower than the values around 4.5 dB found for An Giang.
 449 Figure 7 presents the pixel-based classification accuracy for the An Giang province, calculated

450 from the APP-derived maps, as a function of the retained classification threshold, with a
 451 particular focus on the true optimal threshold, leading to the maximal accuracy, and on the 3dB
 452 threshold. The figure indicates that, for this dataset, a relatively wide range of threshold values -
 453 roughly between 3dB and 5dB in Summer-Autumn, and between 3dB and 7dB in Autumn-
 454 Winter - lead to similarly high pixel-based accuracies. In particular, the use of the baseline
 455 algorithm (3dB threshold) leads to only slightly suboptimal results, with an additional error of
 456 about 2% compared to the optimal accuracy. It was therefore chosen to use the 3dB threshold for
 457 the mapping of rice areas over the whole Mekong delta.

458



459

460 Figure 7. Classification accuracy as a function of the retained classification threshold for season
 461 2 (left) and season 3 (right) in An Giang province. The true optimal threshold t_{opt} , leading to the
 462 maximal accuracy, is calculated and plotted in dashed line, and the baseline 3dB threshold and
 463 corresponding accuracy are plotted in full bold line.

464

465

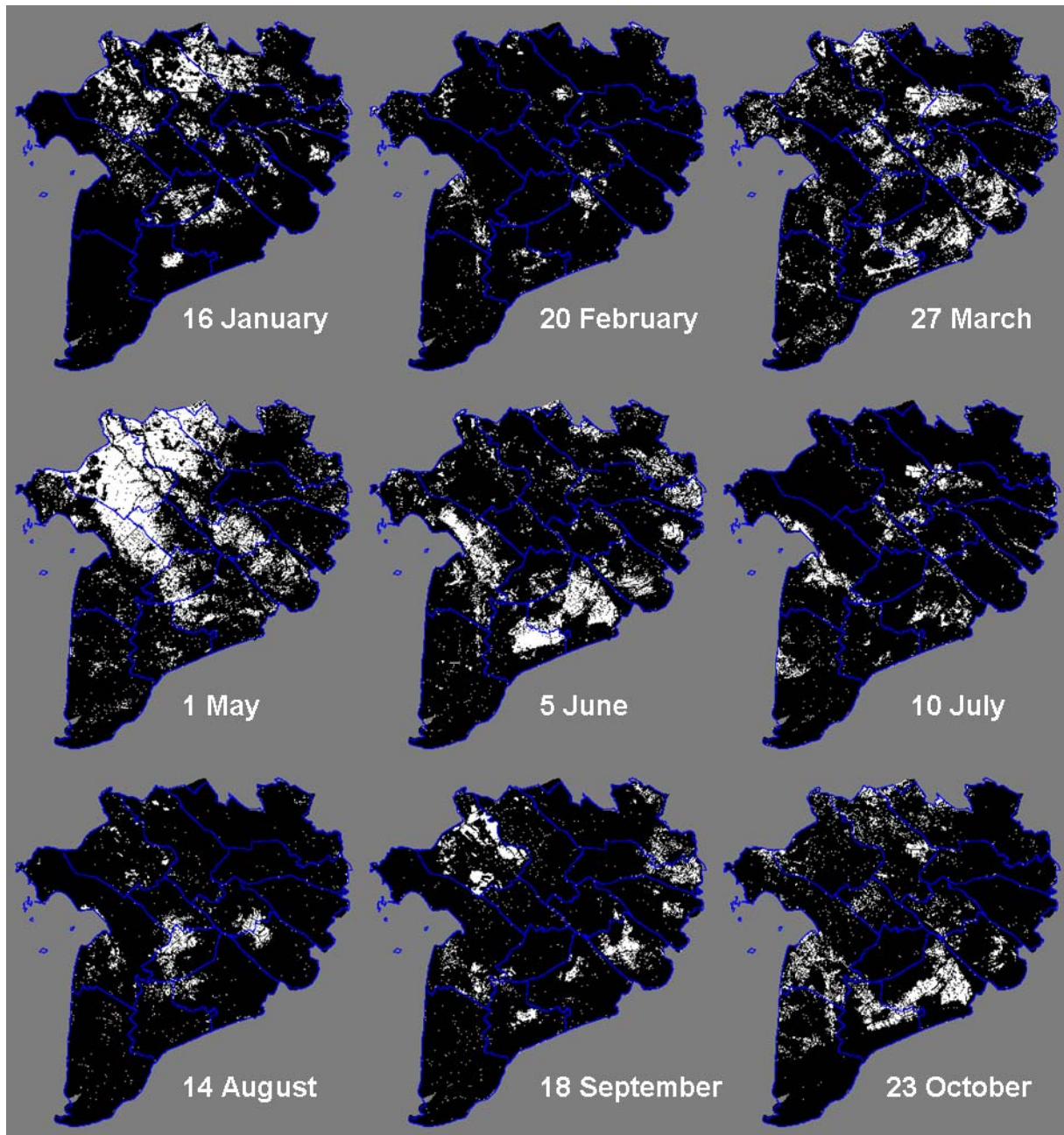
466

467 **D. Creating STC images**

468 Because of the lack of WSM images in the end of 2006, the first crop in 2007 - the Winter-
469 Spring crop – cannot be mapped exhaustively. The study therefore focuses on the other rice
470 seasons. One STC image is created for Season 2 (the Summer-Autumn crop) and another one for
471 Season 3 (i.e. both the main wet season and the Autumn-Winter season because of their
472 simultaneity).

473 In some areas with homogeneous cropping patterns, the simple knowledge of agricultural
474 calendars should be sufficient to select the TC images to be used for the production of the STC
475 images. For the case of the Mekong River Delta however, the variety of cropping patterns and
476 calendars between provinces has to be accounted for. Figure 8 shows intermediate rice maps
477 obtained by considering groups of up to three TC images acquired during a short period of time
478 and belonging to different tracks. The groups are composed of one TC image from track 412
479 together with the preceding TC image from track 304 (seven days before) and the following TC
480 image from track 32 (nine days later) when available, which corresponds to the lines in Table 4.
481 Pixels in white (values above the 3dB threshold for at least one of the TC images in the group)
482 therefore represent the paddy fields that are at the flooding stage around the indicated date. This
483 reflects well the complexity of the cropping patterns in the region, as at each date, flooded fields
484 are present somewhere in the delta. This enhances the need of a precise selection of the TC
485 images at the province level for the production of STC images.

486



487

488

489

490

491

Figure 8. Rice maps derived from nine groups of up to three TC images. Pixels in white represent the pixels with a TC value above the 3 dB threshold for at least one image in the group, and pixels in black with a TC value below the threshold for all the images in the group.

492 In this study, we chose to use time-series of NDVI as ancillary data to select the TC images. The
493 VGT-S10 products of the VEGETATION-2 instrument on-board SPOT-5 have been used. They
494 consist in 10-day syntheses of the four spectral bands of the instrument at a spatial resolution of
495 1km. The NDVI, which is the normalized difference of the near infrared and red reflectances, is
496 a proxy for the chlorophyll content within one pixel, and therefore for the live green vegetation.
497 The 36 VGT-S10 products of the year 2007 covering the Mekong Delta were downloaded and
498 processed to produce NDVI time-series. A cloud-removal filter inspired on the Best Index Slope
499 Extraction (BISE) algorithm (Viovy et al. 1992) was applied on the NDVI time-series. The dates
500 of local crop calendars are estimated by a visual interpretation of the vegetation cycles depicted
501 in the NDVI time-series at selected pure pixels among each province. A sufficient number of
502 pixels should be chosen to represent the cropping pattern diversity in each province (i.e. mainly
503 double and triple cropping) and the variety in each cropping pattern (from early to late crops).

504

505

506 **IV. RESULTS AND DISCUSSION**

507

508 **A. Mapping results**

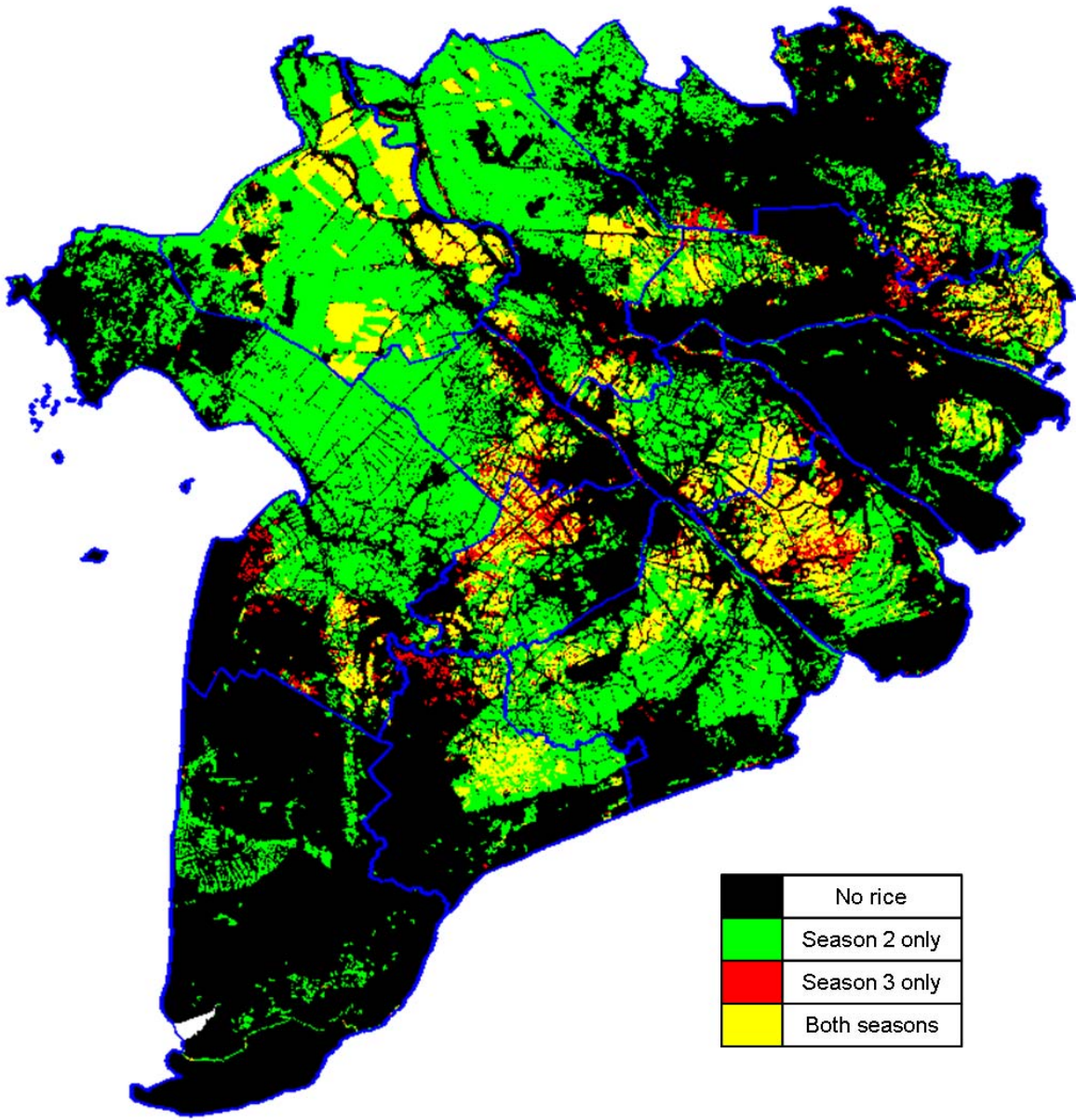
509 A 3dB threshold is applied on the two STC images that have been created by keeping the
510 maximum value of the TC images selected within each province for Season 2 and Season 3. The
511 isolated rice pixels or the very small patches detected as rice (less than 40 pixels) are removed
512 from the rice class because they are likely to be errors due to remaining speckle.

513 Figure 9 shows the rice maps obtained in the whole Mekong delta. The map depicts the areas
514 where rice is grown in Season 2 only in green, in Season 3 only in red, in both seasons in

515 yellow, and the areas where no rice is detected in black. As Season 1 is missing, it is reasonable
516 to assume that in inland provinces, the green areas actually correspond to double-rice patterns
517 and the yellow areas to triple-rice patterns. This map exhibits cropping patterns that are very
518 similar to those presented by (Sakamoto et al. 2006), which include coarser resolution rice maps
519 of 2002 and 2003 derived from MODIS and a land-use map of 2002 provided by the Sub-
520 National Institute for Agricultural Planning and Projection of Vietnam. In particular, in An
521 Giang province, the WSM map illustrates the well-known expansion of triple-rice (labeled as
522 “both seasons” in this case) between 2002-2003 and 2007.

523 Table 5 lists the rice areas for both seasons calculated from these rice maps.

524



525

526

Figure 9. Rice map derived from the STC images for Season 2 and Season 3.

527

528

529

530 **Table 5. Planted area of rice by province (in ha) for Season 2 and Season 3 retrieved from**
 531 **the WSM data**

	Season 2	Season 3
Long An	123461	23817
Tiền Giang	64666	39444
Bến Tre	24531	8981
Trà Vinh	81179	54896
Vĩnh Long	66903	25465
Đồng Tháp	203720	32927
An Giang	263321	78725
Kiên Giang	257890	20120
Cần Thơ	73293	21586
Hậu Giang	56078	36819
Sóc Trăng	155938	28954
Bạc Liêu	67470	26635
Cà Mau	40155	795

532

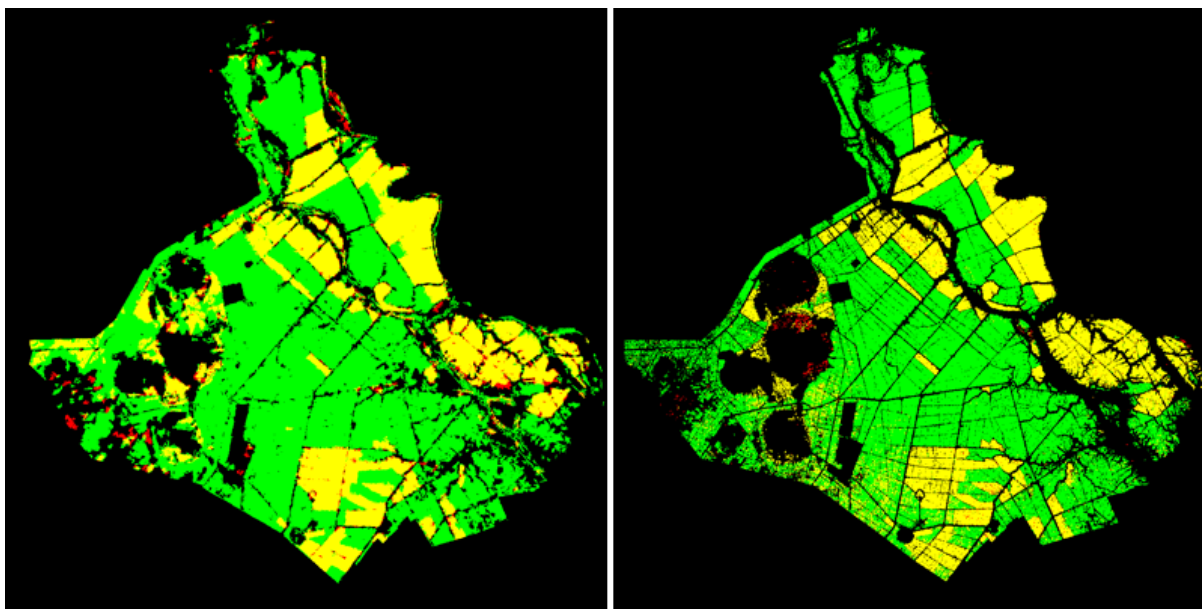
533 **B. Validation**

534 A visual comparison of the rice maps in An Giang is presented in Figure 10 between the new
 535 rice maps derived from WSM and the rice maps derived from APP data in a previous study.
 536 Although the classification features in the two SAR methods are based on different physical
 537 mechanisms, the results compare very well to each other, which demonstrates the robustness of
 538 both methods for the identification of rice fields. The pixel-based accuracy, which corresponds
 539 to the percentage of pixels that are classified in the same category (rice or non-rice) by the two
 540 methods, is equal to 81.3% and 89.5% for Season 2 and Season 3 respectively. When
 541 considering the joint mapping results at the two seasons, four classes are distinguished: no rice,

542 rice in Season 2 only, rice in Season 3 only, and rice in both seasons, similarly to the larger map
543 in Fig. 9. The normalized confusion matrix for the four classes, with the APP map considered as
544 reference data and the WSM map as classification data, is given in Table 6. Each cell in the table
545 contains the percentage of pixels in the scene that are classified in the class defined by its
546 column and by its line in the APP and WSM maps respectively. The overall classification
547 accuracy is therefore equal to the sum of the figures in the diagonal: 75.8%. Most of the
548 classification error is commission error, i.e. pixels classified as non-rice in the APP map are
549 classified as rice in the WSM map (mostly Season 2 and both seasons). Two sources of
550 commission are identified from Fig.10: a) a small part of the rivers are detected as rice by the
551 method based on WSM because the backscattering of water can change with wind conditions,
552 and b) with its coarser spatial resolution, the WSM map is not able to discriminate fine features
553 such as roads and channels between fields. As rivers, roads and channels do not change from
554 year to year, both causes of commission error can be tackled by masking these areas through the
555 use of a GIS land cover database for example.

556

557



558
 559 Figure 10. Rice maps derived from the WSM dataset (left) and APP dataset (right) in An Giang
 560 for Season 2 and Season 3 in 2007 (same legend as Figure 9).

561

562 **Table 6. Confusion matrix between classes derived from APP and WSM.**

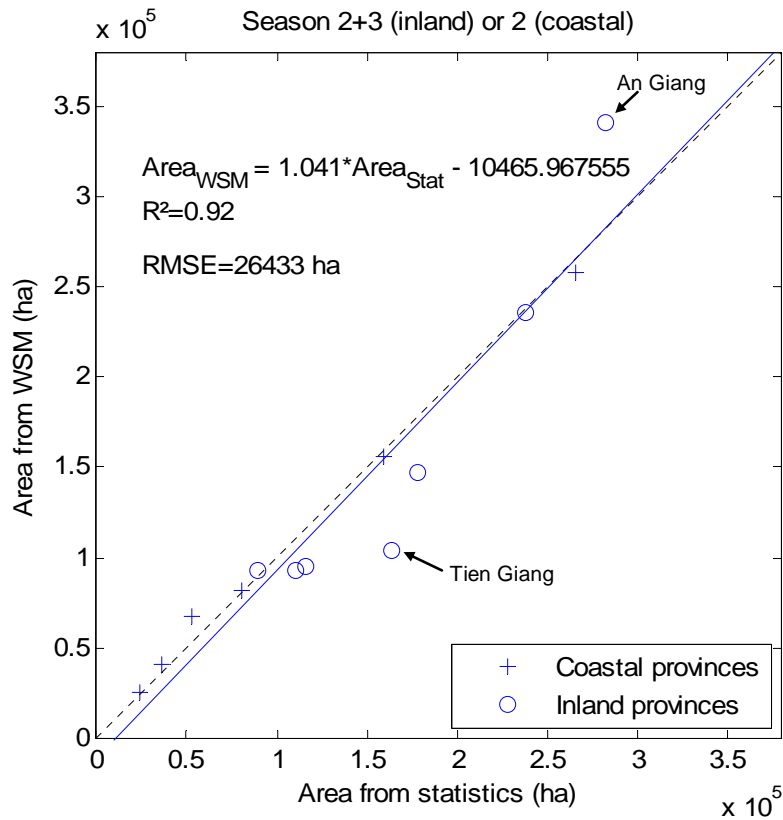
		WSM				
		no rice	season 2	season 3	both seasons	
APP	no rice	19,57%	11,36%	1,51%	4,48%	36,92%
	season 2	1,69%	39,45%	0,12%	1,23%	42,49%
	season 3	0,09%	0,09%	0,03%	0,32%	0,52%
	both seasons	0,34%	2,69%	0,33%	16,71%	20,07%
		21,69%	53,58%	1,98%	22,74%	

563

564 The ability of the new mapping method to retrieve planted areas can be tested against the
 565 statistical data given by GSO. As suggested in Table 3, the planted areas given for the Autumn
 566 category in the statistics has to be compared to the sum of the planted areas retrieved by WSM
 567 for Season 2 and Season 3 in the inland provinces, and to the planted areas retrieved for Season

568 2 in the coastal provinces. The corresponding figures are plotted in Fig. 11. The two datasets
569 show a very good agreement ($R^2=0.92$) with a root mean square error of 26000 ha per province.

570



571

572 Figure 11. Retrieved rice planted areas per province (in ha) for season 2 (coastal provinces) and
573 the sum of Season 2 and Season 3 (inland provinces) vs. statistical rice planted areas in Autumn.

574

The blue line represents the linear regression between the two datasets.

575

576

577 C. Discussion

578 As can be seen from Fig. 11, the area estimation is excellent in coastal provinces and a bit less

579 good in inland provinces. One possible reason for this difference could be that the assumption

580 that the Autumn category from the statistical database contains Season 2 and Season 3 in inland

581 provinces is not totally valid. There might be differences between inland provinces in the
582 definition of seasons by the General Statistics Office. This must not however hide the fact that
583 true sources of error exist. Some sources of error can lead to an overestimation (up to 59000ha in
584 An Giang) or an underestimation (up to 59000ha in Tiền Giang) of the rice planted areas. These
585 sources include the effect of mixed pixels, commission errors (non-rice areas classified as rice)
586 and omission errors (rice areas classified as non-rice).

587 Several types of land use can exhibit a high backscatter increase under certain conditions, thus
588 generating commission errors. These cases can generally be easily discarded by a more detailed
589 analysis of the available SAR time-series. For example, in the Mekong River Delta, a rapid
590 increase in backscatter can happen locally when the seasonal flood recedes, or over permanent
591 water areas (lakes, rivers) because of the wind, resulting in an erroneous detection of rice. The
592 seasonal flood should be relatively easily spotted by detecting low backscatter values during
593 several consecutive repeat-pass acquisitions. Permanent water areas on the other hand can be
594 masked out by applying a threshold on the mean backscatter within a SAR time-series. In the
595 rice growing regions where another major crop is grown (e.g. wheat), confusion could also occur
596 when one image is acquired before harvest and the next one after harvest, which could result in a
597 backscatter increase. But in most cases these crops are not grown simultaneously to rice so the
598 confusion can be avoided by selecting the relevant acquisition dates.

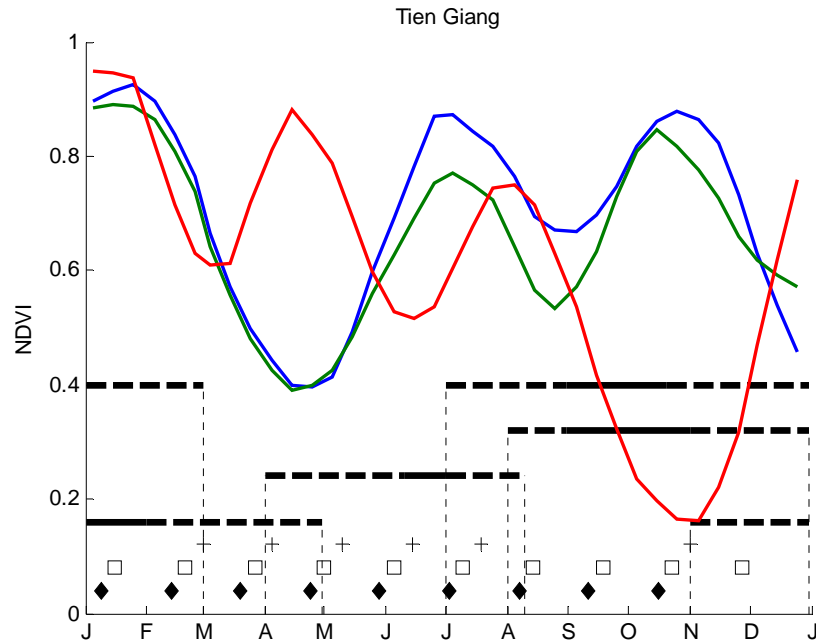
599 The effect of mixed pixels is more important and is directly related to the spatial resolution of
600 the imagery data. In the study area, the agricultural landscape is composed of large surfaces of
601 rice fields separated by smaller non-rice elements such as roads, irrigation channels, dwellings,
602 or vegetable patches, especially in the irrigated areas in the inland provinces. Consequently,
603 many pixels classified as rice actually contain a small proportion of non-rice surface. The

604 reverse is not true, so mixed pixels globally lead to an overestimation of rice planted areas. This
605 overestimation is more important at coarser resolutions, and has already been illustrated in Fig.
606 10 for the An Giang province.

607 The area overestimation due to mixed pixels should also be present in other provinces, but it is
608 not observed in Fig.11. It can be supposed that this overestimation may be at least partially
609 compensated by other error sources that lead to area underestimation, i.e. omission errors. This
610 can happen when SAR data are missing during the few days when the fields are flooded. This is
611 most likely to have happened here for Season 3, when no data could be acquired in track 032.

612 For the extreme case of Tiền Giang, another factor may be involved. The NDVI time-series of
613 three representative selected pixels in the province are plotted in Fig. 12, after smoothing with a
614 central moving average. They all describe a triple-cropping pattern. The green and blue profiles
615 are typical of the well-known Winter-Spring/Summer-Autumn/Autumn-Winter pattern. In the
616 contrary, the red profile differs from this planting scheme, with a peculiar “Spring-Summer”
617 crop (locally named “Xuân Hè”) inserted between the Winter-Spring and Summer-Autumn
618 seasons, and no Autumn-Winter crop as the area is reached by the seasonal floods in October-
619 November. This Winter-Spring/Spring-Summer/Summer-Autumn pattern is reported in (Tanaka
620 1995), only in Tiền Giang province. This minor pattern may be badly detected in the STC
621 images designed for Season 2 and Season 3, and the attribution of each of its three crops to the
622 statistical categories (Spring, Autumn, Winter) is unknown. These two effects combined can
623 explain part of the discrepancies between the WSM and statistical figures in Tiền Giang.

624



625

626

627

628

629

630

631

V. CONCLUSION

632

633

634

635

636

637

638

A novel rice mapping method has been developed, based on former methods using the temporal backscatter change as a classification feature, and adapted to the use of multi-track wide-swath datasets. The effect of the spatial and temporal variation of the incidence angle within the dataset is tackled by using exclusively temporal change images, which are intensity ratio images of two consecutive acquisitions in the same track. This allows increasing significantly the observation frequency and the size of the mapped areas compared to the former methods using single-track narrow-swath datasets.

639 The study has been conducted in the Mekong River Delta, where rice fields have been mapped
640 over the whole delta for two crops in 2007 (Season 2 and Season 3), using ASAR WSM data.
641 Comparison with a rice map of An Giang province produced with finer-resolution data has
642 shown that the rice detection is very effective with the new methods.

643 Regarding area estimation, an excellent correlation has been obtained when comparing the
644 planted areas retrieved from the rice maps to the planted areas reported in the official statistics.
645 However, this positive result is likely to be due partly to error compensation between
646 overestimation and underestimation sources. As such, the operational use of this method for an
647 accurate area estimation of rice fields should be considered only within an integrated scheme
648 involving other data sources. In well-monitored areas where detailed GIS-based land cover maps
649 are available, which is increasingly common, the method can be applied to the sole pixels known
650 to be agricultural areas in order to reduce commission errors and limit the effect of mixed pixels.

651 In that case, the method can be used as a tool to update this GIS land cover database globally
652 and in near-real time much more effectively than by field investigations. Such operational
653 systems can be based on the data provided by the two existing C-band SARs providing wide-
654 swath data, namely ENVISAT/ASAR and RADARSAT-1 and 2. The limiting factor in this case
655 would be data availability. Given the large choice of operating modes for these sensors,
656 acquisition conflicts between users are very frequent and make it difficult to obtain consistent
657 time-series. For example, in this study, it has been possible to use only three satellite tracks,
658 while under these latitudes, each part of the Earth surface can be observed by 6 tracks in
659 ascending pass and 6 in descending pass, which makes a potential observation interval of about
660 3 days. The effective acquisition of this data would require dedicated strategies from the space
661 agencies. In the future, the Sentinel-1 satellite (planned for launch by the European Space

662 Agency around 2012) should be able to solve this problem, and is therefore a very promising
663 tool for the operational application of the rice mapping method developed in this article.

664 Although tested here only in the Mekong River Delta, the method should be efficient in every
665 rice-growing region, as long as a flooding stage is present. New farming practices have
666 developed in the last years in Vietnam, consisting in direct sowing of germinated seeds on wet
667 soil rather than transplanting of young plants in flooded fields. In that case still, fields are
668 flooded a few days after sowing, so the mapping method is still valid, but as the flooding period
669 is reduced, the need of frequent imagery acquisitions is even harsher.

670 As the method is based on the detection of an event that occurs at the beginning of the rice
671 growing cycle, it is well-suited to the early assessment of cultivated areas. Therefore, if
672 successfully applied on an operational basis, it would be potentially very useful to national
673 statistics officers, decision makers and rice trade professionals.

674

675

676 **ACKNOWLEDGEMENT**

677 The ENVISAT/ASAR data used in this study were provided by the European Space Agency
678 (Cat-1 AO project 697).

679

680 **REFERENCES**

681

682 Food and Agriculture Organization of the United Nations, "General status of the system of food
683 and agriculture statistics in Viet Nam", [http://www.faorap-](http://www.faorap-apcas.org/vietnam/No2_VNM_1.pdf)
684 [apcas.org/vietnam/No2_VNM_1.pdf](http://www.faorap-apcas.org/vietnam/No2_VNM_1.pdf)

685 United Nations Department of Economic and Social Affairs, Population Division, "World
686 population to 2300",
687 <http://www.un.org/esa/population/publications/longrange2/WorldPop2300final.pdf>
688 General Statistics Office of Vietnam, "Structure of used land by province",
689 http://www.gso.gov.vn/default_en.aspx?tabid=466&idmid=3&ItemID=6135
690 General Statistics Office of Vietnam, "Agriculture, Fishery and Fishery Statistical Data",
691 http://www.gso.gov.vn/default_en.aspx?tabid=469&idmid=3
692 Food and Agriculture Organization of the United Nations, "FAOSTAT",
693 <http://faostat.fao.org/site/567/default.aspx>
694 Bouvet, A., Le Toan, T., Floury, N., & Macklin, T. (2010). An end-to-end error model for
695 classification methods based on temporal change or polarization ratio of SAR intensities.
696 *IEEE Transactions on Geoscience and Remote Sensing*, 48, 3521-3538
697 Bouvet, A., Le Toan, T., & Lam Dao, N. (2009). Monitoring of the Rice Cropping System in the
698 Mekong Delta Using ENVISAT/ASAR Dual Polarisation Data. *IEEE Transactions on*
699 *Geoscience and Remote Sensing*, 47, 517-526
700 Chakraborty, M., Manjunath, K.R., Panigrahy, S., Kundu, N., & Parihar, J.S. (2005). Rice crop
701 parameter retrieval using multi-temporal, multi-incidence angle Radarsat SAR data.
702 *ISPRS Journal of Photogrammetry & Remote Sensing*, 59, 310-322
703 Chen, C., & McNairn, H. (2006). A neural network integrated approach for rice crop
704 monitoring. *International Journal of Remote Sensing*, 27, 1367-1393
705 Chen, J., Lin, H., & Pei, Z. (2007). Application of ENVISAT ASAR data in mapping rice crop
706 growth in Southern China. *IEEE Geoscience and Remote Sensing Letters*, 4, 431-435

- 707 Frohking, S., Qiu, J., Boles, S., Xiao, X., Liu, J., Zhuang, Y., Li, C., & Qin, X. (2002).
708 Combining remote sensing and ground census data to develop new maps of the
709 distribution of rice agriculture in China. *Global Biogeochemical Cycles*, *16*
- 710 Inoue, Y., Kurosu, T., Maeno, H., Uratsuka, S., Kozu, T., Dabrowska-Zielinska, K., & Qi, J.
711 (2002). Season-long daily measurements of multifrequency (Ka, Ku, X, C, and L) and
712 full-polarization backscatter signatures over paddy rice field and their relationship with
713 biological variables. *Remote Sensing of Environment*, *81*, 194-204
- 714 Kurosu, T., Fujita, M., & Chiba, K. (1995). Monitoring of rice crop growth from space using the
715 ERS-1 C-band SAR. *IEEE Transactions on Geoscience and Remote Sensing*, *33*, 1092-
716 1096
- 717 Le Toan, T., Laur, H., Mougin, E., & Lopes, A. (1989). Multitemporal and dual-polarization
718 observations of agricultural vegetation covers by X-band SAR images. *IEEE*
719 *Transactions on Geoscience and Remote Sensing*, *27*, 709-718
- 720 Le Toan, T., Ribbes, F., Wang, L.-F., Floury, N., Ding, K.-H., Kong, J.A., Fujita, M., & Kurosu,
721 T. (1997). Rice crop mapping and monitoring using ERS-1 data based on experiment and
722 modelling results. *IEEE Transactions on Geoscience and Remote Sensing*, *35*, 41-56
- 723 Liew, S.C., Kam, S.-P., Tuong, T.-P., Chen, P., Minh, V.Q., & Lim, H. (1998). Application of
724 multitemporal ERS-2 synthetic aperture radar in delineating rice cropping systems in the
725 Mekong River Delta, Vietnam. *IEEE Transactions on Geoscience and Remote Sensing*,
726 *36*, 1412-1420
- 727 Lopes, A., Touzi, R., & Nezry, E. (1990). Adaptive speckle filters and scene heterogeneity.
728 *IEEE Geoscience and Remote Sensing Letters*, *28*, 992-1000

- 729 Lopez-Sanchez, J.M., Ballester-Berman, J.D., & Hajnsek, I. (2010). First results of rice
730 monitoring practices in Spain by means of time series of TerraSAR-X dual-pol images.
731 *IEEE Journal of Selected Topics in Applied Earth Observations and Remote Sensing*, in
732 *press*
- 733 Ribbes, F., & Le Toan, T. (1999). Rice field mapping and monitoring with RADARSAT data.
734 *International Journal of Remote Sensing*, 20, 745-765
- 735 Rignot, E., & van Zyl, J. (1993). Change detection techniques for ERS-1 SAR data. *IEEE*
736 *Transactions on Geoscience and Remote Sensing*, 31, 896-906
- 737 Rosenqvist, A. (1999). Temporal and spatial characteristics of irrigated rice in JERS-1 L-band
738 SAR data. *International Journal of Remote Sensing*, 20, 1567-1587
- 739 Sakamoto, T., Nguyen, N.V., Ohno, H., Ishitsuka, N., & Yokozawa, M. (2006). Spatio-temporal
740 distribution of rice phenology and cropping systems in the Mekong Delta with special
741 reference to the seasonal water flow of the Mekong and Bassac rivers. *Remote Sensing of*
742 *Environment*, 100, 1-16
- 743 Shao, Y., Fan, X., Liu, H., Xiao, J., Ross, S., Brisco, B., Brown, R., & Staples, G. (2001). Rice
744 monitoring and production estimation using multitemporal RADARSAT. *Remote*
745 *Sensing of Environment*, 76, 310-325
- 746 Tanaka, K. (1995). Transformation of rice-based cropping patterns in the Mekong Delta: From
747 intensification to diversification. *Southeast Asian Studies*, 33, 363-378
- 748 Viovy, N., Arino, O., & Belward, A. (1992). The Best Index Slope Extraction (BISE): A
749 method for reducing noise in NDVI time-series. *International Journal of Remote*
750 *Sensing*, 13, 1585-1590

- 751 Wang, L.-F., Kong, J.A., Ding, K.-H., Le Toan, T., Ribbes-Baillarin, F., & Floury, N. (2005).
752 Electromagnetic scattering model for rice canopy based on Monte Carlo simulation.
753 *Progress In Electromagnetics Research*, 153-171
- 754 Xiao, X., Boles, S., Froking, S., Li, C., Babu, J.Y., Salas, W., & Moore III, B. (2006). Mapping
755 paddy rice agriculture in South and Southeast Asia using multi-temporal MODIS images.
756 *Remote Sensing of Environment*, 100, 95-113
- 757 Xiao, X., Boles, S., Froking, S., Salas, W., Moore III, B., & Li, C. (2002a). Observation of
758 flooding and rice transplanting of paddy rice fields at the site to landscape scales in
759 China using VEGETATION sensor data. *International Journal of Remote Sensing*, 23,
760 3009-3022
- 761 Xiao, X., Boles, S., Froking, S., Salas, W., Moore III, B., Li, C., He, L., & Zhao, R. (2002b).
762 Landscape-scale characterization of cropland in China using Vegetation and Landsat TM
763 images. *International Journal of Remote Sensing*, 23, 3579-3594
- 764 Xiao, X., Boles, S., Liu, J., Zhuang, D., Froking, S., Li, C., Salas, W., & Moore III, B. (2005).
765 Mapping paddy rice agriculture in southern China using multi-temporal MODIS images.
766 *Remote Sensing of Environment*, 95, 480-492
- 767
- 768